Hydrologic control of carbon cycling and aged carbon discharge in the Congo River basin

Enno Schefuß[1,3], Timothy I. Eglinton[2,3], Charlotte L. Spencer-Jones[4,*], Jürgen Rullkötter[5],

Ricardo De Pol-Holz[6], Helen M. Talbot[4], Pieter M. Grootes[7], Ralph R. Schneider[7,8]

[1]*MARUM – Center for Marine Environmental Sciences, University of Bremen, Germany*

[2]*Department of Geological Sciences, ETH Zürich, Switzerland*

[3]*Department of Marine Chemistry and Geochemistry, Woods Hole Oceanographic Institution, USA*

[4]*School of Civil Engineering and Geosciences, Newcastle University, United Kingdom*

[5]*Institute for Chemistry and Biology of the Marine Environment (ICBM), Carl von Ossietzky University of Oldenburg, Germany*

[6]*GAIA-Antártica, Center for Climate and Resilience Research (CR)[2], Universidad de Magallanes, Punta Arenas, Chile*

[7]*Leibniz-Laboratory for Radiometric Dating and Stable Isotope Research Kiel, Germany, now at: Institute for Ecosystem Research, Christian-Albrechts-University Kiel, Germany*

[8]*Institute for Geosciences, Christian-Albrechts-University Kiel, Germany*

*Now at: Department of Geography, University of Durham, United Kingdom

The age of organic material discharged by rivers provides information about its sources and carbon cycling processes within watersheds. While elevated ages in fluvially-transported organic matter are usually explained by erosion of soils and

21 **sediments deposits[1,2], it is commonly assumed that mainly young organic material is**

22 **discharged from flat tropical watersheds due to their extensive plant cover and rapid**

23 **carbon turnover[3-7]. Here we present compound-specific radiocarbon data of terrigenous**

24 **organic fractions from a sedimentary archive offshore the Congo River in conjunction**

25 **with molecular markers for methane-producing land cover reflecting wetland extent.**

26 **We find that the Congo River has been discharging aged organic matter for several**

27 **thousand years with apparently increasing ages from the Mid- to the Late Holocene.**

28 **This suggests that aged organic matter in modern samples is concealed by radiocarbon**

29 **from atmospheric nuclear weapons testing. By comparison to indicators for past rainfall**

30 **changes we detect a systematic control of organic matter sequestration and release by**

31 **continental hydrology mediating temporary carbon storage in wetlands. As aridification**

32 **also leads to exposure and rapid remineralization of large amounts of previously stored**

33 **labile organic matter we infer that this process may cause a profound direct climate**

34 **feedback currently underestimated in carbon cycle assessments.**

35   Tropical humid ecosystems are hot spots of terrestrial carbon storage[8] and large river

36 systems in tropical areas form an important conduit in the global carbon cycle by transporting

37 vast amounts of biosynthetic OM to the ocean[9,10]. Apparent radiocarbon ages of riverine

38 organic carbon are interpreted as the mean time elapsed since biosynthesis, integrating all

39 intermediate storage, transport and mixing processes, and thus considered to reflect the speed

40 of carbon cycling in watersheds. Radiocarbon studies of fluvially-transported OM reveal

41 relatively young ages in tropical areas[3-7], suggesting rapid carbon turnover, and greater ages in

42 temperate regions with larger influence of geomorphology and soil erosion[1,2]. Among the

43 controlling processes, relative changes in export of contemporary biomass versus erosion of

44 OM from soils or sedimentary rocks (e.g., refs 1,7) as well as storage in intermediate

45   reservoirs, such as floodplains and wetlands (e.g., refs 11-13), are discussed. The exact factors

46   controlling the continental residence times of terrestrial OM in tropical watersheds and their

47   response to climatic changes are, however, not yet fully understood.

48   To provide insight into the response of OM cycling in large tropical watersheds to

49   climatic changes we investigated a sedimentary archive simultaneously recording continental

50   palaeo-climatic changes and variations in terrestrial carbon cycling in the Congo basin.

51   Sediment core GeoB6518-1 (05° 35.30' S, 11° 13.30' E, 962 m water depth, Fig. 1) was

52   recovered from the Congo deep-sea fan close to the river mouth. The Congo is the second

53   largest river on Earth in terms of drainage basin size (about 3.7 x 10^6 km^2), water discharge[14]

54   and terrestrial organic matter export[15]. Located in equatorial Africa, it is characterized by low

55   intra- and inter-annual discharge variability[16]. Steep rapids close to its estuary separate the

56   central Congo basin from sea-level influence. A submarine canyon incises the continental

57   shelf, extending from the Congo estuary and leading to rapid transport of discharged material

58   to the deep-sea fan. The ages of terrestrial organic material are therefore considered to reflect

59   retention processes within the river basin. We measured the ^{14}C content of various OM

60   fractions (total organic matter, microscopic wood fragments, leaf-wax *n*-alkanes, and

61   individual leaf-wax *n*-alcohols) from several depth intervals of core GeoB6518-1 (Table S2).

62   Using the depositional ages based on radiocarbon dating of planktonic foraminifera (Table

63   S1), radiocarbon contents of OM fractions were decay-corrected to derive initial radiocarbon

64   contents. The deviation from the past atmospheric ^{14}C content ($\Delta\Delta^{14}C_{initial}$, see Methods) at the

65   time of deposition can be converted to apparent initial radiocarbon ages. The initial ages of

66   the OM fractions range from isochronous up to 3,000 ^{14}C years (Fig. 2a). Notably, initial ages

67   of wood fragments are contemporaneous to or only slightly older than depositional ages in the

68   Early to Mid-Holocene. In contrast, the plant-wax fractions are older and show higher but

3

69   coherent age variability (Fig. 3). This is in accordance with both a rapid transfer of plant

70   debris through the river system under high discharge conditions and the refractory nature and

71   persistence of plant waxes in soils[17]. The aged terrestrial organic contributions strongly

72   influence the age of total organic carbon (TOC) deposited off the Congo River despite its

73   mixed terrestrial and aquatic origin (Fig. 2a). From about 5,000 years before present (BP) all

74   organic components show a similar trend to greater apparent initial ages towards the present.

75   The Congo River has, thus, exported aged OM for the last several thousand years. This

76   finding is in contrast to ^{14}C results from modern fluvial OM in the Congo River and other

77   tropical river systems, where terrestrial components were found to be mainly contemporary in

78   age[4-7]. We infer that this discrepancy is caused by the influence of radiocarbon from

79   atmospheric nuclear weapons testing in modern samples, masking their original age. This

80   influence is also detected for the uppermost sample from GeoB6518-1 which exhibits

81   reversals in the $\Delta^{14}C_{initial}$ of all OM fractions (Fig. S3). The influence of bomb-derived

82   radiocarbon on modern samples in carbon cycle studies therefore needs to be considered more

83   carefully.

84   To explain the Holocene age variations we investigated indicators for OM contributions

85   from soils, sedimentary rocks and wetlands, and also considered variable carbon turnover due

86   to changes in river transport, continental temperatures and hydrologic conditions. Previously

87   we showed that the OM of core GeoB6518-1 is predominantly terrigenous with the majority

88   derived from soils[18]. The proportion of soil- versus plant-derived OM estimated by the

89   abundance of membrane lipids from soil-hosted bacteria, however, was relatively invariant

90   through time[18] (Table S2). While this suggests that relative contribution changes of soil-

91   derived OM due to variable vegetation cover and soil erosion cannot explain the age

92   variations, it does not rule out erosion of deep soil layers and intermediate deposition and re-

93   suspension during riverine transport as potential processes leading to elevated ages.

94   Nevertheless, we regard these effects as minor considering the relatively flat geomorphology

95   of the Congo basin[14], the Congo's high discharge even under today's relatively dry conditions

96   and the observation that similar age variations were also detected for wood fragments (Fig.

97   2a, 3, 4). Similarly, we rule out an influence of fossil OM contributions from sedimentary

98   rocks as the molecular composition of the plant-wax fractions does not show any indication of

99   thermally mature hydrocarbons (Fig. S1). Also, we infer that hydraulic sorting of fine and

100   coarse particles carrying different radiocarbon contents[5] cannot explain the observed ages as

101   variations were also detected for the coarse (> 150 µm) wood fragments. As no large

102   continental temperature variations in central Africa occurred during the Holocene[19] (Fig. 2b),

103   we also exclude temperature-driven changes in soil carbon turnover[8,20] as an explanation for

104   the observed age variations. Instead, we observe a strong relation to changes in continental

105   hydrology. In particular, the trend towards greater ages from the Mid- to Late Holocene is

106   paralleled by the aridification trend in central Africa[21] (Fig. 2c). Towards the relatively dry

107   present-day conditions all terrestrial OM fractions converge to their greatest initial ages.

108   Comparing the radiocarbon contents of the molecular OM fractions to the hydrogen stable

109   isotope compositions (δD) of the n-C_{24} alcohol as a measure of rainfall intensity[21], reveals that

110   initial ages significantly increased when δD values exceeded -145 ‰ VSMOW, indicating

111   more arid conditions (Fig. 4). We thus conclude that the observed age trend was caused by

112   release of previously stored OM from intermediate reservoirs controlled by changes in

113   continental hydrology. Despite the high coverage of the Congo basin by tropical rainforest,

114   even the deposited wood fragments follow this trend, suggesting a massive release of aged

115   terrestrial OM. Disentangling the sedimentary TOC into pre-aged and fresh portions, i.e.,

116   directly from plants and aquatic organisms, reveals that about 30 to 70 % of TOC is pre-aged

117   during the Early to Mid-Holocene while this portion increases to 70 to 90 % in the Late

118   Holocene (Fig. 2d). Accumulation rates of pre-aged OC at GeoB6518-1 (Fig. 2e) are higher

119   during the latest Holocene than during the wetter Early to Mid-Holocene suggesting strongly

120   increased export fluxes of pre-aged OM by the Congo River under more arid conditions.

121   In order to identify the source of this large-scale old OM release, we analysed bacterial

122   signature lipids, i.e., bacteriohopanepolyols (BHPs)[22,23], in sediments of GeoB6518-1. In

123   particular, we focused on 35-aminobacteriohopane-30,31,32,33,34-pentol (aminopentol), a

124   marker for aerobic methanotrophic bacteria predominant in wetlands[22]. Strong similarities of

125   the BHP signature in the Congo deep-sea fan and in wetland deposits[22,23] (Fig. S2), coupled

126   with limited ^{13}C depletion of the BHPs, are consistent with aerobic oxidation of methane in a

127   terrestrial setting[23] (see supplement). The aminopentol abundance profile in GeoB6518-1

128   (Fig. 2f) reveals a striking resemblance to the continental hydrologic changes[21] (Fig. 2c). In

129   the humid Early Holocene, maximum abundance of aminopentol indicates largest wetland

130   extent in the Congo basin while its decreasing abundance suggests shrinking methane-

131   producing land cover during the Mid- to Late Holocene concomitant with increasing initial

132   ages of terrestrial OM (Fig. 2a). The observed threshold-like age trend with decreasing

133   rainfall intensity (Fig. 4) may point to an environmental tipping point with respect to wetland

134   extent depending on the regional geomorphology of the basin. The most likely candidate for

135   such a wetland system is the Cuvette Congolaise in the vast central depression of the Congo

136   basin at the confluence of several tributaries. It hosts one of the World's largest swamp forests

137   containing seasonally and permanently flooded wetlands with an estimated area of 360,000

138   km^2 (ref 24) (Fig. 1). These wetlands receive plant OM from local and upstream sources and

139   accumulate substantial amounts of OM[25,26]. Having remained largely unnoticed until

140   recently[27,28], the modern central Congo basin is estimated to store at least 9 Pg C[28] as a

141   consequence of water-saturated wetland soils inhibiting aerobic OM decomposition and

6

142 instead resulting in (slower) anaerobic degradation emitting methane and other greenhouse

143 gases[29].

144   These various lines of evidence suggest that areas of OM storage under anoxic

145 conditions and associated methane production in the central Congo basin were more extended

146 during the more humid Early Holocene, serving as an important locus of temporary storage of

147 plant biomass. More rainfall in the basin led to higher transport of plant organic material into

148 the Cuvette Congolaise where it accumulated in the vast permanently flooded swamp forest

149 areas. In water-logged wetland soils remineralisation is diminished leading to enhanced

150 preservation and storage of OM. The elevated ages of refractory plant-wax lipids even under

151 wet, high discharge conditions point to additional processes, such as intermediate storage

152 during fluvial transport and /or deep soil erosion, affecting their ages. Upon aridification,

153 permanently flooded wetland areas with methane-producing land cover contracted and

154 previously anoxic deposits eroded triggering release of aged terrestrial OM. Additionally,

155 lower water levels caused erosion of deeper soil layers and previously deposited river beds.

156 Exposure of OM previously stored under anoxic conditions not only leads to release of

157 refractory organic components which are discharged but also of labile OM that is rapidly

158 oxidized. Thus, in addition to decreasing carbon sequestration due to wetland shrinkage, the

159 release and remineralisation of labile OM introduces a direct climatic feedback under more

160 arid conditions, the magnitude of which remains uncertain. Given that most tropical

161 watersheds, such as the Amazon[27], contain extended wetland areas these findings have

162 profound global implications for the response of tropical terrestrial carbon inventories and

163 carbon cycle feedbacks upon hydrological changes. Impacted by natural climatic changes as

164 well as anthropogenic activities such as land use, deforestation, rising CO_2 levels and

165 associated effects on climate[30], any changes in tropical wetland extent may thus exert a direct

166   climatic feedback. Presently, such effects are underestimated in global climate assessments[30]

167   and must be considered to more accurately assess the response of terrestrial carbon cycle

168   dynamics to future climatic change.

169

170 **References**

171   1   Raymond, P. A. & Bauer, J. E. Riverine export of aged terrestrial organic matter to the

172   North Atlantic Ocean. *Nature* **409**, 497-500 (2001).

173   2   Hilton, R. G. *et al.* Climatic and geomorphic controls on the erosion of terrestrial

174   biomass from subtropical mountain forest. *Glob. Biogeochem. Cycles* **26**,

175   doi:10.1029/2012gb004314 (2012).

176   3   Hedges, J. I. *et al.* Organic carbon-14 in the Amazon River system. *Science* **231**, 1129-

177   1131 (1986).

178   4   Martin, E. E. *et al.* Age of riverine carbon suggests rapid export of terrestrial primary

179   production in tropics. *Geophys.Res. Lett.* **40**, 5687-5691 (2013).

180   5   Spencer, R. G. M. *et al.* An initial investigation into the organic matter

181   biogeochemistry of the Congo River. *Geochim. Cosmochim. Acta* **84**, 614-627 (2012).

182   6   Galy, V. & Eglinton, T. Protracted storage of biospheric carbon in the Ganges-

183   Brahmaputra basin. *Nature Geosci.* **4**, 843-847 (2011).

184   7   Marwick, T. R. *et al.* The age of river-transported carbon: A global perspective. *Glob.*

185   *Biogeochem. Cycles* **29**, GB004911 (2015).

186   8   Carvalhais, N. *et al.* Global covariation of carbon turnover times with climate in

187   terrestrial ecosystems. *Nature* **514**, 213-217 (2014).

188   9   Huang, T. H., Fu, Y. H., Pan, P. Y. & Chen, C. T. A. Fluvial carbon fluxes in tropical

189   rivers. *Curr. Opin. Environ. Sustain.* **4**, 162-169 (2012).

190   10 Schluenz, B. & Schneider, R. R. Transport of terrestrial organic carbon to the oceans

191   by rivers: re-estimating flux- and burial rates. *Int. J. Earth Sci.* **88**, 599-606 (2000).

192   11 Blair, N. E., Leithold, E. L. & Aller, R. C. From bedrock to burial: the evolution of

193   particulate organic carbon across coupled watershed-continental margin systems. *Mar.*

194   *Chem.* **92**, 141-156 (2004).

195   12   Kusch, S., Rethemeyer, J., Schefuß, E. & Mollenhauer, G. Controls on the age of

196   vascular plant biomarkers in Black Sea sediments. *Geochim. Cosmochim. Acta* **74**,

197   7031-7047 (2010).

198   13   Drenzek, N. J. *et al.* A new look at old carbon in active margin sediments. *Geology* **37**,

199   239-242 (2009).

200   14   Runge, J. The Congo River, Central Africa. in *Large Rivers: Geomorphology and*

201   *Management*   (ed A. Gupta) 293-309 (Wiley, 2007).

202   15   Coynel, A., Seyler, P., Etcheber, H., Meybeck, M. & Orange, D. Spatial and seasonal

203   dynamics of total suspended sediment and organic carbon species in the Congo River.

204   *Glob. Biogeochem. Cycles* **19**, GB4019 (2005).

205   16   Laraque, A., Bricquet, J. P., Pandi, A. & Olivry, J. C. A review of material transport

206   by the Congo River and its tributaries. *Hydrol. Process.* **23**, 3216-3224 (2009).

207   17   Huang, Y., Li, B., Bryant, C., Bol, R. & Eglinton, G. Radiocarbon dating of aliphatic

208   hydrocarbons: a new approach for dating passive-fraction carbon in soil horizons. *Soil*

209   *Sci. Soc. Am. J.* **63**, 1181-1187 (1999).

210   18   Weijers, J. W. H., Schouten, S., Schefuss, E., Schneider, R. R. & Sinninghe Damsté, J.

211   S. Disentangling marine, soil and plant organic carbon contributions to continental

212   margin sediments: A multi-proxy approach in a 20,000 year sediment record from the

213   Congo deep-sea fan. *Geochim. Cosmochim. Acta* **73**, 119-132 (2009).

214   19   Weijers, J. W. H., Schefuss, E., Schouten, S. & Sinninghe Damsté, J. S. Coupled

215   thermal and hydrological evolution of tropical Africa over the last deglaciation.

216   *Science* **315**, 1701-1704 (2007).

217   20   Davidson, E. A. & Janssens, I. A. Temperature sensitivity of soil carbon

218   decomposition and feedbacks to climate change. *Nature* **440**, 165-173 (2006).

219 21 Schefuß, E., Schouten, S. & Schneider, R. R. Climatic controls of Central African

220   hydrology during the last 20,000 years. *Nature* **437**, 1003-1006 (2005).

221 22 Spencer-Jones, C. L. *et al.* Bacteriohopanepolyols in tropical soils and sediments from

222   the Congo River catchment area. *Org. Geochem.* **89-90**, 1-13 (2015).

223 23 Talbot, H. M. *et al.* Variability in aerobic methane oxidation over the past 1.2 Myrs

224   recorded in microbial biomarker signatures from Congo fan sediments. *Geochim.*

225   *Cosmochim. Acta* **133**, 387-401 (2014).

226 24 Bwangoy, J. R. B., Hansen, M. C., Roy, D. P., De Grandi, G. & Justice, C. O. Wetland

227   mapping in the Congo Basin using optical and radar remotely sensed data and derived

228   topographical indices. *Remote Sens. Environ.t* **114**, 73-86 (2010).

229 25 Mitsch, W. J. *et al.* Wetlands, carbon, and climate change. *Landsc. Ecol.* **28**, 583-597

230   (2013).

231 26 Kayranli, B., Scholz, M., Mustafa, A. & Hedmark, A. Carbon storage and fluxes

232   within freshwater wetlands: a critical review. *Wetlands* **30**, 111-124 (2010).

233 27 Keddy, P. A. *et al.* Wet and wonderful: The World's largest wetlands are conservation

234   priorities. *Bioscience* **59**, 39-51 (2009).

235 28 Joosten, H. & Tapio-Biström, M.-L. Peatlands - guidance for climate change

236   mitigation through conservation, rehabilitation and sustainable use. in *Mitigation of*

237   *climate change in agriculture* Vol. 5   100 pp. (Food and Agriculture Organization of

238   the United Nations/Wetlands International, Rome, 2012).

239 29 Borges, A. V. *et al.* Globally significant greenhouse-gas emissions from African

240   inland waters. *Nature Geosci.* **8**, 637-642 (2015).

241 30 Arneth, A. *et al.* Terrestrial biogeochemical feedbacks in the climate system. *Nature*

242   *Geosci.* **3**, 525-532 (2010).

243

244

Correspondence and requests for materials

246   Correspondence and requests for materials should be addressed to E.S.

247   (eschefuss@marum.de).

248

Author contributions

261   E.S., T.I.E., J.R., P.M.G., and R.R.S. designed the study. Analytical work was performed by

262   E.S., C.L.S.-J., H.M.T., J.R., P.M.G., and R.D.P.-H.. E.S. wrote the manuscript approved by

263   all co-authors.

264

265 **Competing financial interests**

266 The authors declare no competing financial interests.

267

Figure captions

Figure 1: The Congo River basin in central Africa. Redrawn after ref 14. Light grey areas are lakes. Dark grey area is the present-day extent of swamp forest in the Cuvette Congolaise[24,27]. Black star offshore the Congo River mouth is sampling location of sediment core GeoB6518-1.

Figure 2: OM ages offshore the Congo River and central African environmental changes. a) Offsets in radiocarbon contents versus the past atmosphere and apparent initial ages at time of deposition (brown: wood pieces, green: n-C$_{24}$ alcohol, grey: n-alkanes, blue: TOC), error bars show analytical uncertainty propagated with $\Delta^{14}C_{atm}$ uncertainty, b) estimates of past temperatures[19], c) hydrogen stable isotope composition of n-C$_{29}$ alkane[21] reflecting rainfall intensity, green dots: n-C$_{24}$ alcohol, error bars show analytical uncertainty, d) TOC disentangled in fresh (green) and pre-aged (brown) portions, e) accumulation rate of pre-aged OC, f) abundance of aminopentol reflecting extent of methane-producing landcover[23].

Figure 3: Correlation of age variations between different OM fractions. Initial radiocarbon offsets are strongly correlated (r = 0.93, p < 0.05) for n-alkanes (grey dots) and n-C$_{24}$ alcohol indicating that both are affected by the same continental retention processes. Error bars show analytical uncertainty propagated with $\Delta^{14}C_{atm}$ uncertainty. Radiocarbon offsets are more negative for n-alkanes than for n-C$_{24}$ alcohol indicating that n-alkanes are more refractory than n-C$_{24}$ alcohol. Radiocarbon

14

291 offsets of wood fragments (brown dots) show no correlation to initial radiocarbon

292 offsets of n-C$_{24}$ alcohol except for the lowest initial radiocarbon offsets, i.e., highest

293 apparent initial ages.

294

295 **Figure 4: Relation between rainfall intensity and OM ages.** Comparison of initial

296 radiocarbon offsets of wood pieces (brown dots) and n-C$_{24}$ alcohol (green dots) with

297 hydrogen isotope compositions of n-C$_{24}$ alcohol. Error bars show analytical

298 uncertainty propagated with $\Delta^{14}C_{atm}$ uncertainty. Initial radiocarbon offsets of n-

299 alkanes (Fig. 3) and TOC show the same trend but are omitted for clarity. Where the

300 hydrogen stable isotope composition of the n-C$_{24}$ alcohol exceeds -145 ‰ VSMOW,

301 initial radiocarbon offsets of all OM fractions become more negative indicating

302 release of previously stored, i.e., pre-aged, material.

303

304   **Online Content** Methods are available in the online version of the paper; references unique to

305   this section appear only in the online paper. Source data and additional display items are in

306   the Supplementary Information.

307

308   **Methods**

309   **Age model of GeoB6518-1.** The age model of GeoB6518-1 is based on AMS dating of mixed

310   planktonic foraminifera containing *Globigerinoides ruber* (white), *Globigerinoides sacculifer*

311   and *Orbulina universa* isolated from sediments by wet-sieving (> 150 µm) and picking.

312   Fractions were cleaned with H_2O and 15% H_2O_2, carbonate was converted to CO_2 with 100%

313   phosphoric acid and subsequently catalytically reduced to graphite for AMS measurement of

314   radiocarbon (^{14}C) contents. ^{14}C contents were corrected for blank effects[31] (Table S1). Most

315   foraminiferal ages were reported earlier[21] and re-calibrated to calendar ages in this study. An

316   additional age point was added for depth 128-138 cm. A further sample (78-88 cm) was lost

317   during AMS measurement. All dates were calibrated with Calib7.0 using the Marine13

318   radiocarbon age calibration and no regional and temporal offset in the reservoir age

319   correction[32]. We set the mid-point of the sampling interval to the mean age of the calibrated 2-

320   σ age interval. Because the uppermost sample (5-15 cm) contains radiocarbon from

321   atmospheric nuclear weapons testing (post-1950 age), we set the core-top to zero age and did

322   not regard the uppermost sample as an age tie-point. Ages of individual samples between tie-

323   points were linearly interpolated.

324   **Radiocarbon dating of total organic carbon and wood fragments**. Total organic carbon

325   (TOC) contents (Tables S2, S3, S4) were determined by combustion of ground and de-

326   carbonated sediment samples at 1050°C using a Leco CS230 Carbon-Sulphur analyser. The

327   relative precision of the measurements, based on triplicate analyses was better than 1.8%

328   relative standard deviation. For ^{14}C analyses of TOC, ground sediments were treated with 1%

329   hydrochloric acid to remove carbonates and subsequently freeze-dried. Samples were

330   combusted with copper oxide and silver wool in quartz tubes and the CO_2 released converted

331   into graphite for AMS measurement. ^{14}C contents were corrected for blank contributions[31].

332   Several microscopic wood fragments (> 150 μm) were isolated from each sediment sample

333   under a binocular microscope. After acid-base-acid treatment to remove humic materials they

334   were combusted and the resulting CO_2 catalytically converted to graphite for ^{14}C

335   measurement by AMS. ^{14}C contents were corrected for blank contributions and small sample

336   size[33]. Two samples (253-258 cm, 453-458 cm) yielded ages of wood pieces younger than

337   depositional ages. This may be due to slight variations in the marine reservoir age. Therefore,

338   their corresponding ^{14}C data were omitted from further calculations. As these data derive from

339   deglacial and early Holocene samples, omitting them from discussion has no influence on the

340   observation of increasing wood ages towards the Late Holocene. Data are listed in

341   supplementary Table S2.

342   **Radiocarbon dating of plant-waxes.** Sediments were Soxhlet-extracted with a 93:7 mixture

343   of dichloromethane and methanol and afterwards saponified with 0.5 M KOH in methanol.

344   After re-extraction with hexane, neutral fractions were separated by liquid chromatography

345   over silica-gel (SiO_2) columns into apolar, ketone and polar fractions by elution with hexane,

346   hexane/dichloromethane and methanol, respectively. Elemental sulphur was removed from

347   apolar fractions using activated copper before branched and cyclic lipids were removed by

348   urea adduction. Unsaturated compounds were removed by liquid chromatography over

349    $AgNO_3$-impregnated SiO_2 columns. *n*-Alkane fractions were quantified against external

350   alkane standards via gas chromatography-flame ionisation detection (GC-FID) and

351   quantitatively transferred into quartz tubes, combusted and the produced CO_2 catalytically

352   converted into graphite before AMS measurement. Alcohol fractions were acetylated with

353   acetic anhydride with known isotopic composition and treated by urea adduction and $AgNO_3$-

354   SiO_2 chromatography. After GC-FID quantification, the *n*-C_{24} alcohol was isolated by

355   preparative gas chromatography using a gas chromatograph coupled to a preparative fraction

356   collector[34]. After cleaning the isolated compounds by silica-gel column chromatography,

357 aliquots were checked for purity by GC-FID and samples were transferred into quartz tubes,

358 combusted and the produced CO_2 catalytically converted into graphite for AMS measurement.

359 ^{14}C contents were corrected for modern and fossil blank contributions to small samples by

360 error propagation. n-Alcohol radiocarbon contents were corrected for carbon contribution

361 from the added acetate group by mass balance calculation. The hydrogen isotope ratio of the

362 n-C_{24} alcohol was measured using a mass spectrometer connected to a gas chromatograph via

363 a pyrolysis interface against H_2 reference gas. The H_3-factor was measured daily and was < 6

364 ppm mV^{-1} with variability from day to day of less than 0.2 ppm mV^{-1}. Analyses of an external

365 alkane standard ("Arndt B", Arndt Schimmelmann, Indiana State University) revealed a mean

366 absolute precision of 3 ‰ and an accuracy of 0 ‰. Precision of δD composition of the n-C_{24}

367 alcohol is based on replicate analyses. The δD value of the n-C_{24} alcohol was corrected for the

368 added acetate group by mass-balance calculation. Data are listed in supplementary Table S2.

369 **Calculation of initial $\Delta\Delta^{14}C$ and apparent initial ages.** If the depositional age is known, i.e.,

370 the calendar age derived from the planktonic foraminifera, it is possible to calculate the initial

371 radiocarbon content from the measured fraction modern (Fm) of all OM AMS results (Table

372 S2) using the following equation[35]:

373 $$\Delta^{14}C_{inital} = (Fm\ e^{(\lambda t)} - 1) \times 1000\ ‰$$

374 Fm is the measured fraction modern, λ is the decay constant (1/8267 years^{-1}) of ^{14}C, and

375 t is time since deposition in years. For the sampling depth for which the foraminiferal [14]C

376 sample was lost (78-88 cm), we assumed the depth-integrated age from the linear

377 interpolation (2492 ± 354 calendar years) as depositional age in order to be able to calculate

378 initial radiocarbon contents of different OM fractions.

379 The offset of the initial radiocarbon contents of OM fractions to that of the past

380 atmosphere ($\Delta^{14}C_{atm}$) is calculated as:

381         $\Delta\Delta^{14}C_{initial} = \Delta^{14}C_{initial} - \Delta^{14}C_{atm}$

382    $\Delta^{14}C$ values for the past atmosphere are based on time-integrated values derived from the

383   Intcal13 southern Hemisphere atmospheric data[36]. For the uppermost sample (5-15 cm),

384   which contains nuclear bomb-derived radiocarbon, we obtained the atmospheric ^{14}C content

385   from the atmospheric measurements[37] at the year of core retrieval (year 2000 CE). The

386   associated error for this sample was obtained from the corresponding ages of the sample depth

387   interval[37]. $\Delta^{14}C_{atm}$ values are given in Table S2.

388   In order to provide ages instead of only radiocarbon contents, the apparent initial

389   (conventional) ^{14}C age is calculated from the initial radiocarbon content[35]:

390   ^{14}C age = -8033 x ln [(1 + $\Delta^{14}C_{initial}$/1000)/(1 + $\Delta^{14}C_{atm}$/1000)] ^{14}C years

391   with $\Delta^{14}C_{initial}$ the initial radiocarbon content of each OM fraction and $\Delta^{14}C_{atm}$ the atmospheric

392   radiocarbon content at the time of deposition.

393   **Estimates of pre-aged OC fractions and accumulation rates.** To provide estimates of the

394   relative and absolute release of previously deposited, i.e., aged, organic matter, we conducted

395   a mass-balance calculation using the amount and initial ^{14}C contents of TOC and the initial

396   ^{14}C contents of plant-wax n-alkanes and of the past atmosphere (Table S2) to disentangle

397   fresh from pre-aged portions within TOC.

398   Pre-aged OC % = TOC % x ($\Delta^{14}C_{TOC\_initial} - \Delta^{14}C_{atm}$) / ($\Delta^{14}C_{alkanes\_initial} - \Delta^{14}C_{atm}$)

399   with TOC = TOC content of sample, $\Delta^{14}C_{TOC\_initial}$ = decay-corrected past ^{14}C contents of

400   TOC, $\Delta^{14}C_{atm}$ = past atmospheric ^{14}C contents, $\Delta^{14}C_{alkanes\_initial}$ = decay-corrected past ^{14}C

401   contents of n-alkanes (all data in Table S2).

402   The n-alkanes as oldest dated fractions in all sediment samples were taken as representing the

403   age of released organic material acknowledging that also these compounds contain fresh

404   portions, i.e., directly derived from plants. As TOC also contains aquatic OM of modern

405   origin albeit in small amounts[18] which adds to the estimated fresh portion of TOC this results

406   in a slight over-estimation of the fresh, directly plant-derived OM. Additionally, it must be

19

407   considered that the labile OM, which is released from wetland deposits, is rapidly oxidised

408   (see main text) and will not be preserved in sedimentary archives. The estimates of pre-aged

409   sedimentary TOC portions therefore reflect minimum estimates of released organic matter.

410   To evaluate if not only the relative portion of pre-aged OC in the sedimentary archive

411   increased but also the absolute flux of pre-aged material, we calculated the accumulation rate

412   of pre-aged OC in the sediment given by the percentage of pre-aged OC multiplied by the

413   bulk sediment accumulation rate (bulk accumulation rate = sedimentation rate x dry bulk

414   density). While we acknowledge that the accumulation rates of all sedimentary components

415   are strongly dominated by the sedimentation rate (see supplementary Fig. S3d) it is clear that

416   the accumulation rate of pre-aged OC in the latest Holocene exceeds its values during the

417   Early and Mid-Holocene suggesting that also the export flux of pre-aged OC by the Congo

418   River is higher under most arid conditions.

419   **Influence of fossil plant-wax contributions.** In order to evaluate if the higher plant-wax ages

420   were caused by variable admixture of fossil, i.e., petrogenic, contributions, we calculated the

421   Carbon Preference Index (CPI)[38]:

422    $CPI = 0.5 \times (\Sigma(C_i + C_{i+2} + .. + C_n) / \Sigma(C_{i-1} + C_{i+1} + .. + C_{n-1}) + \Sigma(C_i + C_{i+2} + .. + C_n) / \Sigma(C_{i+1} +$

423    $C_{i+3} + .. + C_{n+1}))$

424   where i is the number of carbon atoms. CPI was calculated for *n*-alkanes ranging from i = 27

425   to n = 33 and for *n*-alcohols from i = 22 to n = 28. Terrestrial higher plants produce long-chain

426   *n*-alkanes with elevated CPI values[38] whereas thermally altered and extensively degraded

427   organic matter contains *n*-alkanes with a CPI around 1 (ref 39). CPI indices of *n*-alkanes and

428   *n*-alcohols do not correlate with their initial radiocarbon content (see supplementary Fig. S1).

429   Therefore, we rule out that the observed age variations reflect contributions of petrogenic

430   material from eroded sedimentary rocks.

431   **Bacteriohopanepolyols.** Full details of the BHP methodology were published previously[23,40].

432   Briefly, total lipids were extracted from freeze-dried sediments using a modified Bligh and
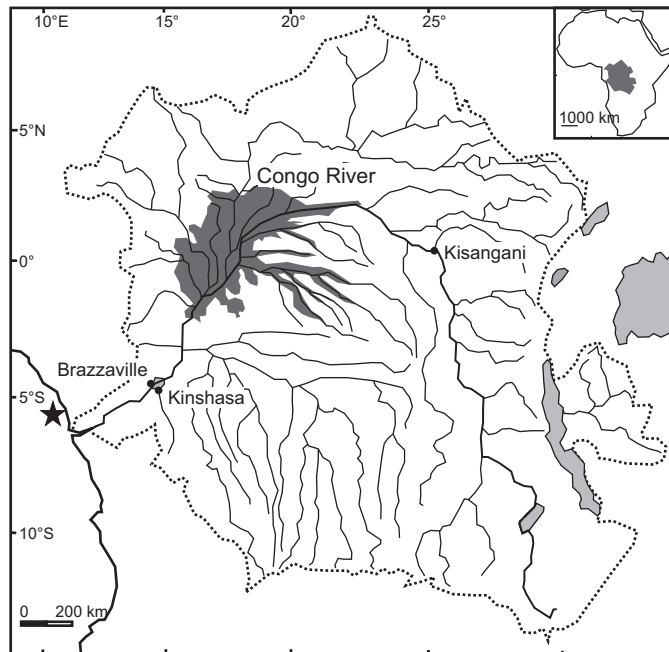
433   Dyer technique. One third of the extract was then acetylated to yield acetylated BHPs, which

434   were analysed by reversed-phase high performance liquid chromatography-atmospheric

435   pressure chemical ionisation-mass spectrometry (HPLC-APCI-MS^n). Semi-quantification of

436   BHP contents was achieved employing the characteristic base peak areas of individual BHPs

437   in mass chromatograms relative to the *m/z* 345 mass chromatogram base peak area of the

438   acetylated 5α-pregnane-3β,20β-diol internal standard. Averaged relative response factors

439   relative to the internal standard, determined from a suite of acetylated BHP standards, were

440   used to adjust the BHP peak areas. Typical error in absolute quantification was ± 20%, based

441   on selected replicate analyses and BHP standards of known concentration[23,40]. BHP data are

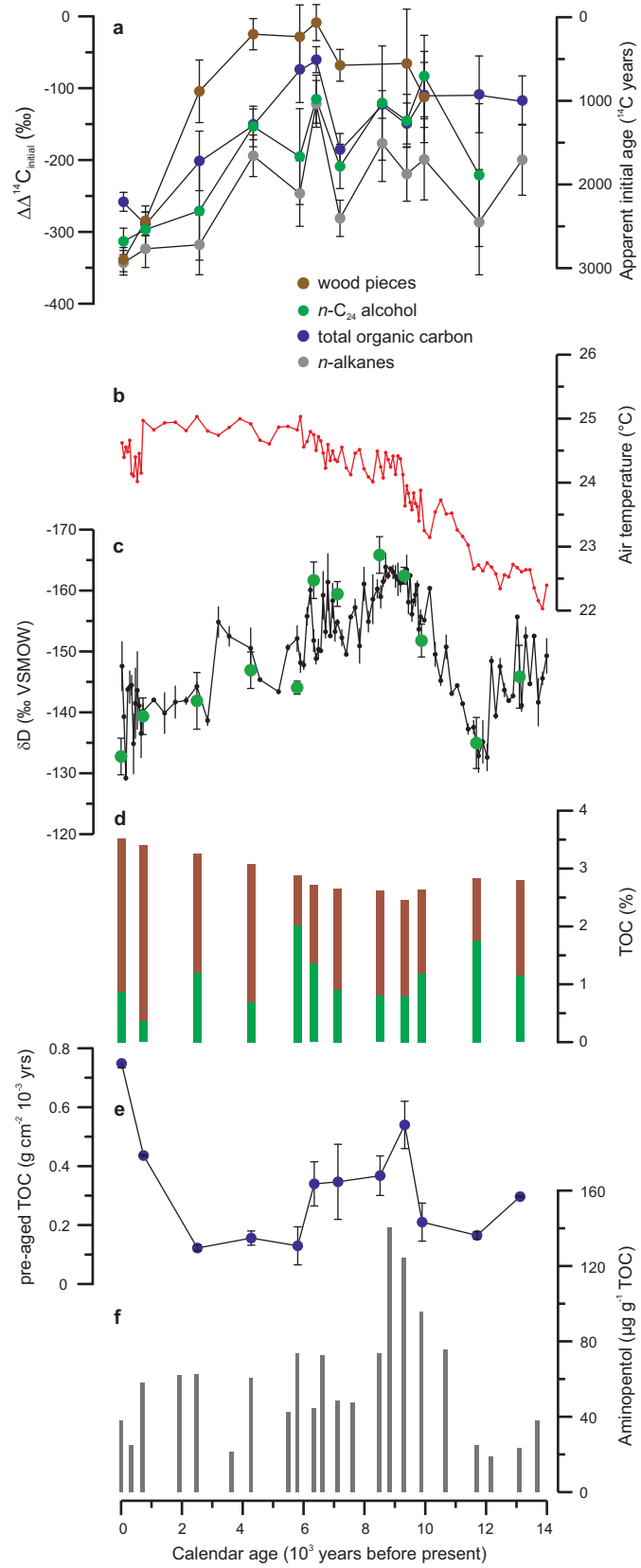442   in supplementary tables S3, S4 and supplementary figure S2.

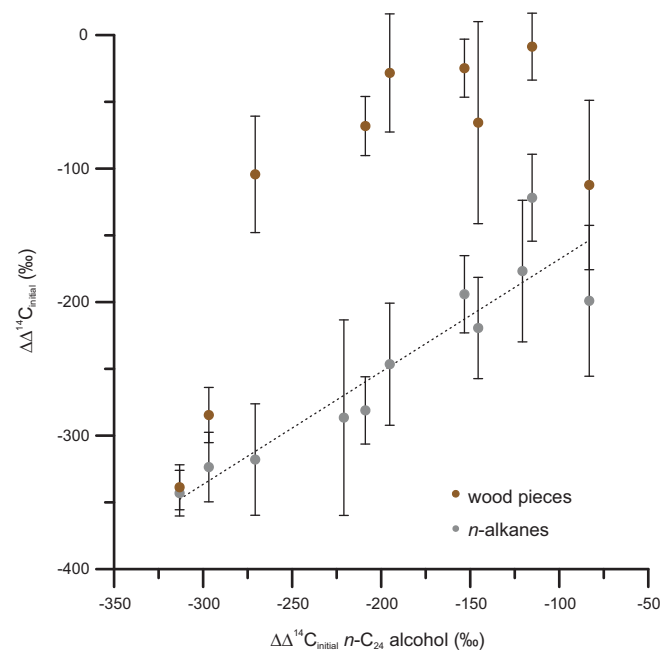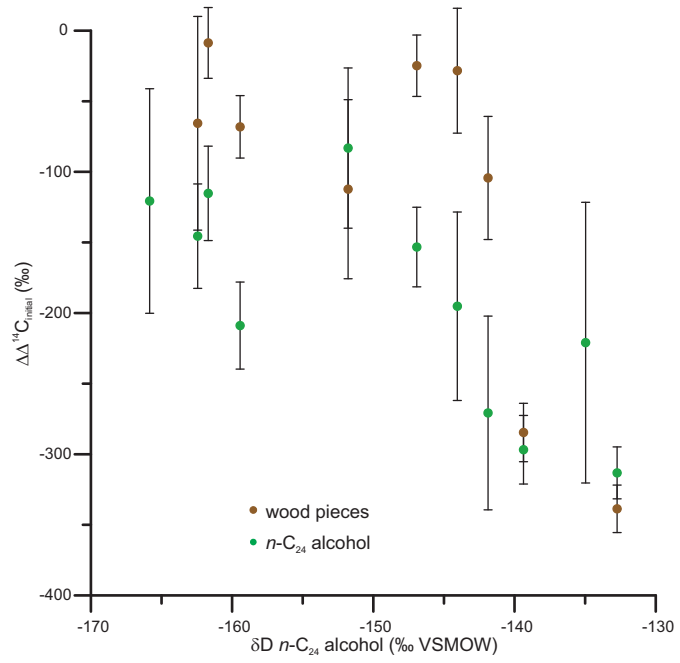443   **Data availability.** Data generated in this study are available from the PANGAEA database

444   (https://doi.pangaea.de/10.1594/PANGAEA.862021).

445

References only in Methods

31   Nadeau, M.-J. *et al.* Sample throughput and data quality at the Leibniz-Labor AMS facility. *Radiocarbon* **40**, 239-245 (1998).

32   Reimer, P. J. *et al.* INTCAL13 and MARINE13 radiocarbon age calibration curves 0-50,000 years cal BP. *Radiocarbon* **55**, 1869-1887 (2013).

33   Santos, G. M., Southon, J. R., Griffin, S., Beaupre, S. R. & Druffel, E. R. M. Ultra small-mass AMS C-14 sample preparation and analyses at KCCAMS/UCI Facility. *Nucl. Instrum. Methods Phys. Res. B* **259**, 293-302 (2007).

34   Eglinton, T. I., Aluwihare, L. I., Bauer, J. E., Druffel, E. R. M. & McNichol, A. P. Gas chromatographic isolation of individual compounds from complex matrices for radiocarbon dating. *Anal. Chem.* **68**, 904-912 (1996).

35   Stuiver, M. & Polach, H. A. Discussion: Reporting of ^{14}C data. *Radiocarbon* **19**, 355-363 (1977).

36   Hogg, A. G. *et al.* SHCAL13 southern hemisphere calibration, 0-50,000 years cal BP. *Radiocarbon* **55**, 1889-1903 (2013).

37   Levin, I., Kromer, B. & Hammer, S. Atmospheric Delta (CO2)-C-14 trend in Western European background air from 2000 to 2012. *Tellus Ser. B* **65**, 20092 (2013).

38   Eglinton, G. & Hamilton, R. J. Leaf epicuticular waxes. *Science* **156**, 1322-1335 (1967).

39   Peters, K. E. & Moldowan, J. M. *The Biomarker Guide: Interpreting Molecular Fossils in Petroleum and Ancient Sediments.* (Prentice-Hall, 1993).

40   van Winden, J. F. *et al.* Bacteriohopanepolyol signatures as markers for methanotrophic bacteria in peat moss. *Geochim. Cosmochim. Acta* **77**, 52-61 (2012).
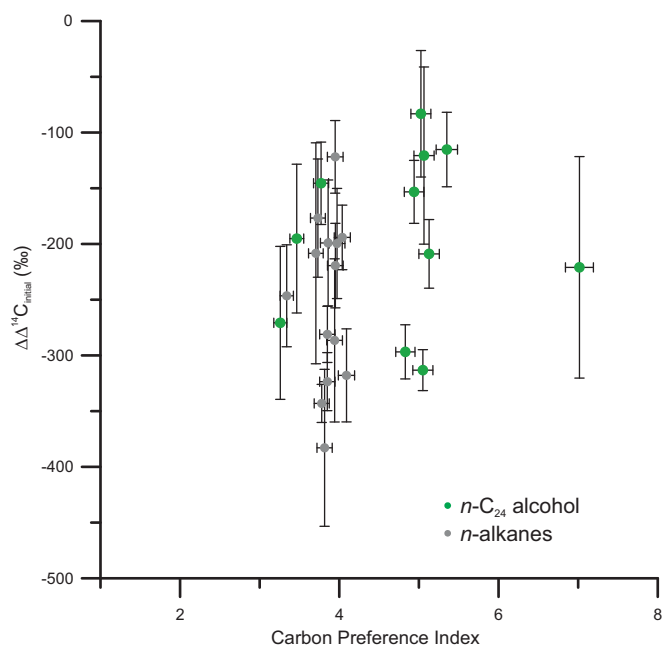
10°E	15°	20°	25°	

5°N

Congo River

0°   Kisangani

Brazzaville
5°S   Kinshasa

10°S

0   200 km

1000 km

a

- wood pieces
- n-C_{24} alcohol
- total organic carbon
- n-alkanes

b

c

d

e

f

$\Delta\Delta^{14}C_{initial}$ (‰)

Apparent initial age (^{14}C years)

Air temperature (°C)

δD (‰ VSMOW)

TOC (%)

pre-aged TOC (g cm^{-2} 10^{-3} yrs)

Aminopentol (µg g^{-1} TOC)

Calendar age (10^3 years before present)

Figure S1: Absence of fossil OM influences on OM ages. Initial radiocarbon offsets of *n*-alkanes (grey dots) and *n*-C$_{24}$ alcohol (green dots) versus their respective Carbon-Preference-Indices (CPI), error bars show analytical uncertainty propagated with $\Delta^{14}C_{atm}$ uncertainty.
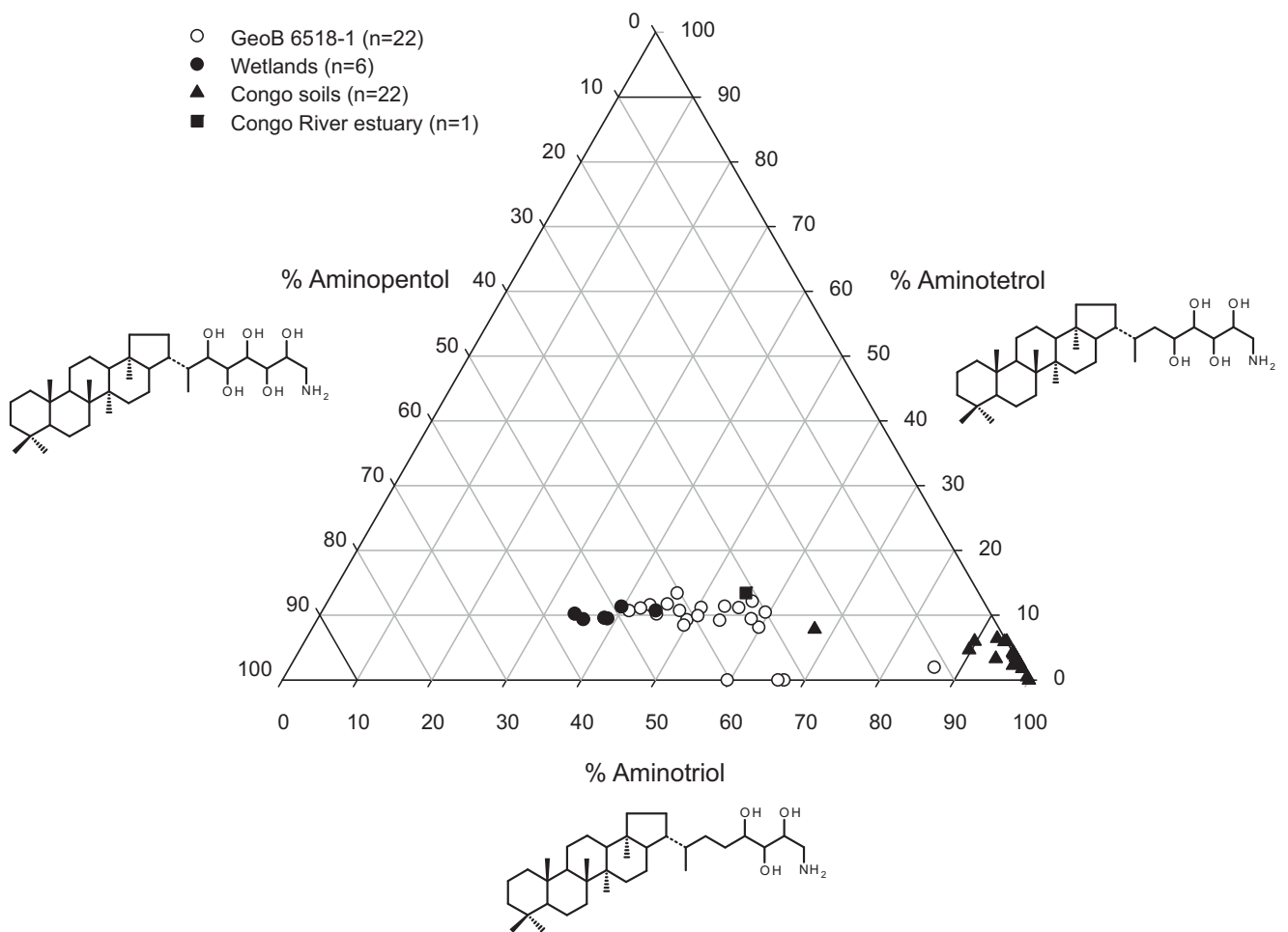
Figure S2: BHP compositions of Congo wetland deposits, soils, and sediments. Ternary plot of the relative abundance of aminoBHP compounds (aminotriol, aminotetrol and aminopentol) present in core GeoB6518-1 (22 samples; this study), the Congo estuarine sediment, 6 wetland sediments and 22 soils from the Congo (data from ref 23).
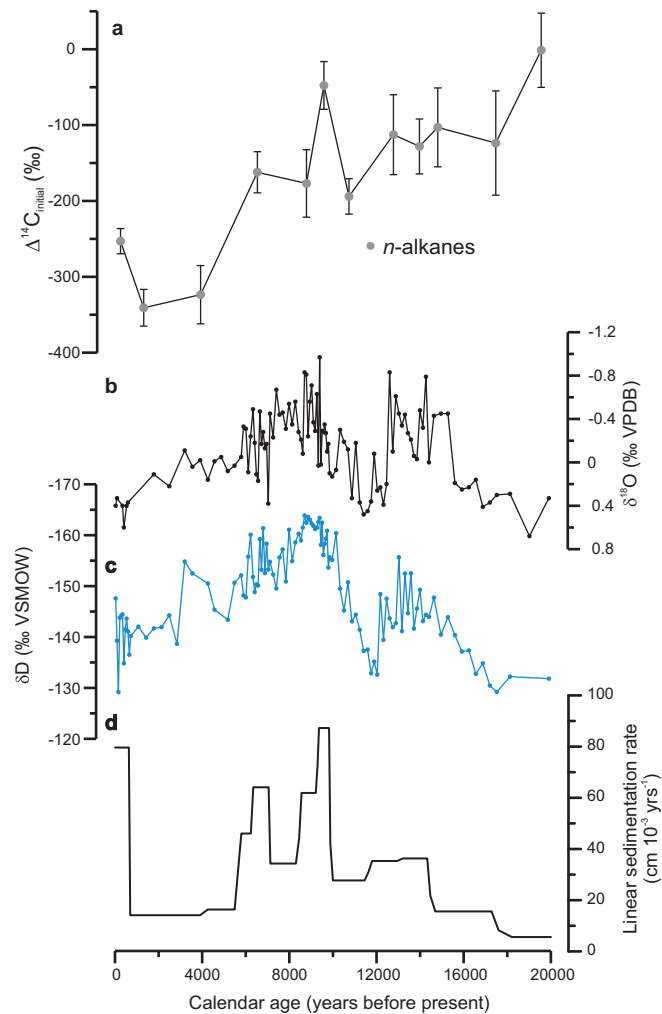
Figure S3: Independence of OM ages, proxy records and sedimentation.
Comparison of initial radiocarbon contents of *n*-alkanes in GeoB6518-1 (a) with
Congo River runoff reconstructions based on oxygen isotope compositions of
planktonic foraminifera (b, black), compound-specific plant-wax based
reconstruction of rainfall intensity in the Congo basin[21] (c, blue) and linear
sedimentation rate of GeoB6518-1 (d). Error bars in a) reflect analytical
uncertainty.